Rotational, Steric, and Coriolis Effects on the F + HCl → HF + Cl Reaction on the $1^2A'$ Ground-State Surface†

Paolo Defazio and Carlo Petrongolo*

Dipartimento di Chimica, Università di Siena, Via A. Moro 2, I-53100 Siena, Italy and Istituto per i Processi Chimico-Fisici del CNR, Via G. Moruzzi 1, I-56100 Pisa, Italy

Received: December 3, 2008; Revised Manuscript Received: January 21, 2009

We present a quantum study of the reaction $F(^2P) + HCl(X^1\Sigma^+) \rightarrow HF(X^1\Sigma^+) + Cl(^2P)$ on a recently computed $1^2A'$ ground-state surface, considering HCl in the ground vibrational state, with up to 16 rotational quanta j_0. We employ the real wavepacket (WP) and flux methods for calculating coupled-channel (CC) and centrifugal-sudden (CS) initial-state probabilities up to $J = 80$ and 140, respectively. We also report CC and CS ground-state cross sections and CS excited-state cross sections and discuss the dynamics analyzing WP time evolutions. The HCl rotation highly enhances reaction probabilities and cross sections, as it was previously found for probabilities at $J \leq 4$. CS errors depend on j_0, on its z projection K_0, and on the collision energy and are small at $j_0 = 0$ and 16 but large at $j_0 = 8$. Differences between CC and CS results are associated with the reaction stereodynamics and energetics. Steric effects favor indeed the overcoming of the potential barrier and a linearly dominated mechanism. Attractive Coriolis couplings favor instead the energy flow from the HCl rotation to the F−H---Cl reactive vibration. WP snapshots confirm and explain the HCl rotational effects, because the density into the nearly collinear F−H---Cl product channel increases remarkably with j_0. Finally, our CS rate constant is underestimated with respect to the experiment, pointing out the need of more accurate multisurface and CC calculations.

1. Introduction

The reaction $F(^2P) + HCl(X^1\Sigma^+) \rightarrow HF(X^1\Sigma^+) + Cl(^2P)$ is involved in the chemistry of hydrogen halide lasers and is an important example of heavy−light−heavy dynamics, and its reactants and products correlate via the $1^2A'$, $2^2A'$, and $1^2A''$ FHCl potential-energy surfaces (PES). This reaction was experimentally and theoretically investigated in refs 1−9, for example. Würzberg et al.[1] and Moore et al.[2] thus measured the thermal rate constant from 139 to 373 K. Sayós et al.[3] calculated an ab initio PUMP2/6-311G(3d2f,3p2d) PES, with a barrier height of 0.174 eV. This value was then empirically reduced to 0.049 eV for reproducing the observed rate, through variational-transition-state-theory calculations.[3] This PES was then employed in quasi-classical-trajectory[4] (QCT) and split-operator[5] studies.

In 2006, Deskevich et al.[6] (DHTSN) reported a high-level, ab initio $1^2A'$ ground-state PES, obtained via multireference configuration interaction and Davidson correction calculations, complete basis set extrapolation of aug-cc-pVnZ data, and energy scaling to reproduce the experimental exothermicity. This PES has a transition state at $F\hat{H}Cl = 123.5°$, a barrier height of 0.165 eV, and is exothermic by 1.486 eV. Including zero-point energies (ZPE), the barrier is reduced to 0.147 eV. Although the DHTSN PES was obtained through external scaling and without spin−orbit coupling, it improves remarkably that of Sayós et al.[3]

Three subsequent theoretical studies of the reaction dynamics employed the DHTSN PES.[7−9] Hayes et al.[7] thus reported QCT and quantum-mechanical (QM) time-independent reaction probabilities for HCl in the ground vibrational state, at total angular momentum $J = 0$, reactant rotation $j_0 \leq 15$, product vibration $v' \leq 3$, and rotation $j' \leq 12$. They also presented coupled-channel (CC) probabilities for $J \leq 4$ and at 0.204 eV above the reactant ground-state energy. These authors found that the HCl rotation increases strongly the reaction probabilities and discussed this behavior via a QCT model. Zolot et al.[8] and Quéméner et al.[9] then performed QCT and QM calculations on the DHTSN PES, investigating product distributions and ultracold reactivity, respectively.

Extending the HDNTS work,[7] we here report QM CC and centrifugal sudden (CS) initial-state-resolved probabilities at high J values, CC and CS ground-state cross sections, and CS excited-state cross sections. Within the Born−Oppenheimer (BO) approximation, we employ the $1^2A'$ DHTSN PES and a time-dependent, real wavepacket (WP) method, and we also discuss the reaction mechanism through WP snapshots. We shall not present a full dynamical study, which is very computer demanding for F + HCl. Indeed, it also requires the knowledge of the $2^2A'$ and $1^2A''$ PESs that interact nonadiabatically with the $1^2A'$ one and of the associated rovibronic and spin−orbit coupling surfaces. We describe our method in section 2, report probabilities and cross sections in section 3, analyze the WP time evolution in section 4, and close with our conclusions in section 5.

2. Method

We calculated initial-state-resolved reaction probabilities $P^{Jp}_{j_0K_0}(E_{col})$ for HCl in the ground vibrational state, using the real WP and flux formalisms,[10,11] *sinc* initial WPs,[12] and reactant Jacobi coordinates R, r, and γ. Here J is the total angular momentum, $p = \pm$ is the parity, j_0 and $K_0 = \boldsymbol{R}\cdot\boldsymbol{j}_0$ are the initial rotational quanta of HCl, E_{col} is the collision energy, and $\gamma = 0$ corresponds to the collinear F−H−Cl. Following the results

† Part of the George C. Schatz Festschrift.

* To whom correspondence should be addressed. E-mail: petrongolo@unisi.it.

10.1021/jp8106414 CCC: $40.75
Published on Web 03/04/2009

TABLE 1: Parameters of the Calculations[a]

sinc initial WP		
translational energy center	0.3 eV	
R center and width α	16 and 20	
smoothing parameter β	0.1	
R range and number of grid points	2−21	359
r range and number of grid points	1.5−17	359
no. of associated Legendre polynomials		120
potential and centrifugal cutoff	0.44	
R and *r* absorption start at	18 and 14	
R and *r* absorption strength	0.01	
flux analysis at *r*	13	

[a] Values in au, unless otherwise specified.

of some tests, which showed that high values of $K = \boldsymbol{R}\cdot\boldsymbol{j}$ inhibit the reactivity, CC calculations have been performed with $K \leq 8$, which is enough for converging probabilities up to $E_{col} = 0.8$ eV.

This reaction must be studied employing a large rotational−vibrational basis, implying that CC calculations are very time consuming. After many tests, we converged $P_0^{\,0\,0}{}^{+}$ with the parameters and basis of Table 1, using 15 465 720 functions at $J = 0$. Varying the dimensions of the radial grid and of the Legendre basis, we checked that probabilities are converged up to $E_{col} = 0.8$ eV. However, using this large basis, CC calculations at any $J \leq 140$, which are necessary for converging cross sections at $j_0 > 0$ and up to 0.4 eV, are outside our present computer facilities. We therefore calculated CC probabilities at $J = 0$, 20, 40, 60, and 80, $p = +$, $j_0 = 0$, 8, and 16, and $K_0 \leq 4$. Of course, CC cross sections at $j_0 > 4$ are not converged with $K_0 \leq 4$, but we here present only the well-converged ground-state cross section.

CS probabilities were also calculated at $J = 100$, 120, and 140 and at other j_0 and K_0 values, up to 10.

For obtaining cross sections $\sigma_{j_0}(E_{col})$, we approximate other partial-wave probabilities via the following *J*-shifting technique.[13−15] As usual, CC and CS probability thresholds are shifted with *J* and K_0, and we fit these shifts as

$$S_{j_0K_0}^{Jp} = a_{j_0K_0}^{Jp}J + b_{j_0K_0}^{Jp}J^2 + c_{j_0K_0}^{Jp}K_0^2 \qquad (1)$$

If CC or CS probabilities P^{J_1} and P^{J_2} are known and $J \in [J_1,J_2]$, we then estimate P^J via the linear interpolation

$$P_{j_0K_0}^{Jp}(E_{col}) \approx P_{j_0K_0}^{J_1p}\left[E_{col} - \left(S_{j_0K_0}^{Jp} - S_{j_0K_0}^{J_1p}\right)\right]\frac{J_2 - J}{J_2 - J_1} + P_{j_0K_0}^{J_2p}\left[E_{col} + \left(S_{j_0K_0}^{J_2p} - S_{j_0K_0}^{Jp}\right)\right]\frac{J - J_1}{J_2 - J_1} \qquad (2)$$

The comparison with some CC or CS data shows that this approach gives good results for probabilities and cross sections.

3. Probabilities and Cross Sections

We present in Figure 1 some CC and CS probabilities $P_{j_0}^{J\,+}$ at $J = 0$, 20, and 80, $p = +$, $j_0 = 0$, 8, and 16, and $K_0 = 0$. These results point clearly out the dominant role of the HCl rotational excitation on the reaction dynamics.

In fact, probabilities at $j_0 = 8$ and 16 are much larger than those at $j_0 = 0$. For example, at $J = 80$ and $E_{col} = 0.8$ eV, we obtain CC $P_{0\,0}^{80\,0}{}^{+} = 0.05$, $P_{8\,0}^{80\,0}{}^{+} = 0.33$, and $P_{16\,0}^{80\,0}{}^{+} = 0.66$, i.e., an increase up to ∼13 times. Moreover, the probability-threshold shifts $({}^{thr}E_{j_0}^{J\,+} - {}^{thr}E_{j_0}^{0\,+})$ decrease at high j_0 quanta. At $J = 80$,

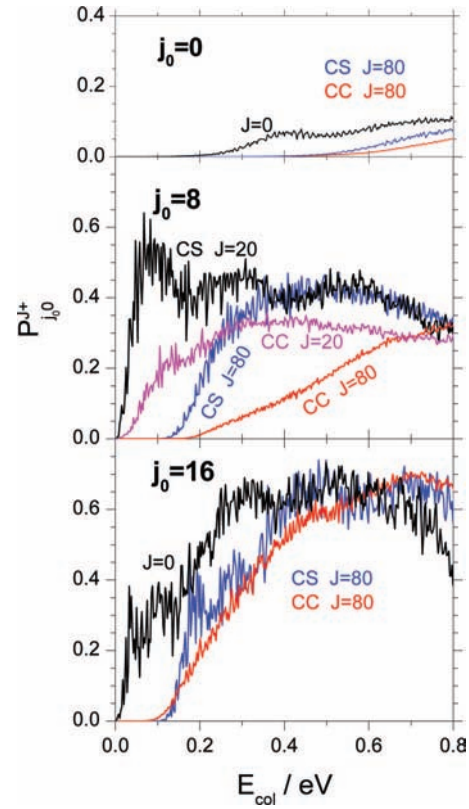

Figure 1. (Top) CC and CS probabilities $P_{0\,0}^{J\,+}$ at $J = 0$ and 80, $p = +$, $j_0 = 0$, and $K_0 = 0$. (Middle) CC and CS probabilities $P_{8\,0}^{J\,+}$ at $J = 20$ and 80, $p = +$, $j_0 = 8$, and $K_0 = 0$. (Bottom) CC and CS probabilities $P_{16\,0}^{J\,+}$ at $J = 0$ and 80, $p = +$, $j_0 = 16$, and $K_0 = 0$.

e.g., these shifts are equal to ∼0.25, ∼0.17, and ∼0.07 eV at $j_0 = 0$, 8, and 16, respectively. This implies that the reactivity enhancement due to the HCl rotation exceeds the inhibition associated with the HCl centrifugal barrier, proportional to $j_0(j_0 + 1)$.

Contrasting CC and CS probabilities, we find that the results are dependent on j_0. The upper and lower panels of Figure 1 show indeed an acceptable or good agreement between CC and CS probabilities at $j_0 = 0$ or 16, respectively, and up to $J = 80$. As usual, CS results present more resonances, because they are not averaged on *K*. On the contrary, CS probabilities of the middle part of Figure 1, at $j_0 = 8$ and $K_0 = 0$, are highly overestimated with respect to the CC ones, at low and intermediate E_{col}, whereas they agree better at higher energies.

A semiclassical picture of the rotational dynamics gives a possible explanation of this finding and some insights on the reaction stereodynamics, showing that the low-energy reactivity is larger when K_0 and/or $K = 0$. In fact, $j_0 > 0$ and $K_0 = 0$ imply that $\boldsymbol{j}_0$ is orthogonal to F−Cl and then to the FHCl plane, because the rotational angular momentum is always orthogonal to H−Cl. The H atom thus initially rotates in the triatomic plane, moving preferentially near the minimum energy path, with the barrier at $\gamma^{\ddagger} = 56.5°$, and attaching the incoming F atom, driven by the HF + Cl exothermicity. On the contrary, H leaves the FHCl plane if $K_0 > 0$ and eventually rotates in a plane orthogonal to F−Cl when $K_0 = j_0$. This corresponds to $\gamma = 90°$, i.e., to a nonreactive orientation. In the CS approximation, $K_0 = 0$ is conserved, and the reaction is more favored than in the CC dynamics, when all *K* values are possible. On the other hand, many *K* channels are open at higher E_{col}, and the negative Coriolis couplings thus increase the CC reactivity, which becomes more similar to the CS one. Note that the HCl

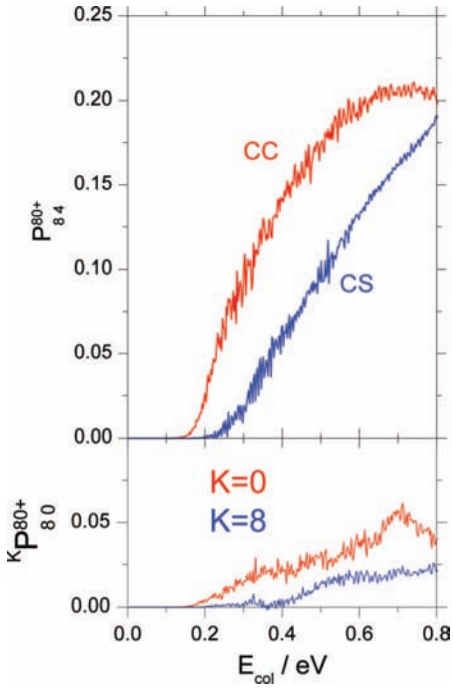

Figure 2. (Top) CC and CS probabilities $P^{80}_{8\,4}{}^{+}$ at $J = 80$, $p = +$, $j_0 = 8$, and $K_0 = 4$. (Bottom) CC probabilities $^{K}P^{80}_{8\,0}{}^{+}$ at $J = 80$, $p = +$, $j_0 = 8$, $K_0 = 0$, and $K = 0$ and 8.

rotational level at $j_0 = 16$ is above the ZPE-corrected barrier. Therefore, the good CC-CS agreement at $j_0 = 16$ could be also due to less important K steric effects at this initial excitation.

In the upper part of Figure 2 we plot CC and CS probabilities $P^{80}_{8\,4}{}^{+}$ at $J = 80$, $p = +$, $j_0 = 8$, and $K_0 = 4$. At these initial conditions, the CC reactivity is now larger than the CS one. These results, and their comparison with those at $K_0 = 0$, confirm our previous analysis on the role of K. The CS dynamics occurs indeed with constant $K_0 = 4$, which lowers the probability with respect to that at $K_0 = 0$. On the contrary, Coriolis couplings open also the reactive $K = 0$ channel, increasing the probability above the CS one but however below than that at $K_0 = 0$. Note also the lower CC threshold, due to the attractive Coriolis couplings, and the slight enhancement of the low-energy probabilities with respect to those at $K_0 = 0$, owing to the entrance centrifugal term $[J(J + 1) - 2K_0^2]/(2\mu_{F+HCl}R^2)$.

The K role is also confirmed by K-projections $^{K}P^{80}_{8\,0}{}^{+}$ of the CC probability on the $|K\rangle$ Wigner states, which we plot in the lower panel of Figure 2, at $J = 80$, $p = +$, $K_0 = 0$, and $K = 0$ and 8. We obtain similar results at $K_0 > 0$. We see that K inhibits the reactivity, which is larger at $K = 0$ and decreases at higher K values, when F follows a less reactive path toward Cl.

In conclusion, the reaction probabilities depend on the interplay between rotational, steric, and energetic effects. A low collisional or rotational energy, steric effects are more important and the reaction is favored by a dynamics with K_0 and/or $K = 0$. On the other hand, Coriolis effects dominate the reaction mechanism at higher energies, coupling rotations, and vibrations via a rotational-to-vibrational energy transfer.

We contrast CC and CS ground-state cross sections σ_0 in the upper panel of Figure 3. Note that these $j_0 = 0$ cross sections are converged up to $E_{col} = 0.8$ eV with $J \leq 80$, as the upper panel of Figure 1 shows. The threshold is at ~0.15 eV, i.e., near the zero-point-energy barrier of 0.147 eV, implying a negligible H-atom tunneling below the barrier. In agreement with probabilities of the upper part of Figure 1, we see that the CS result is slightly overestimated with respect to and more

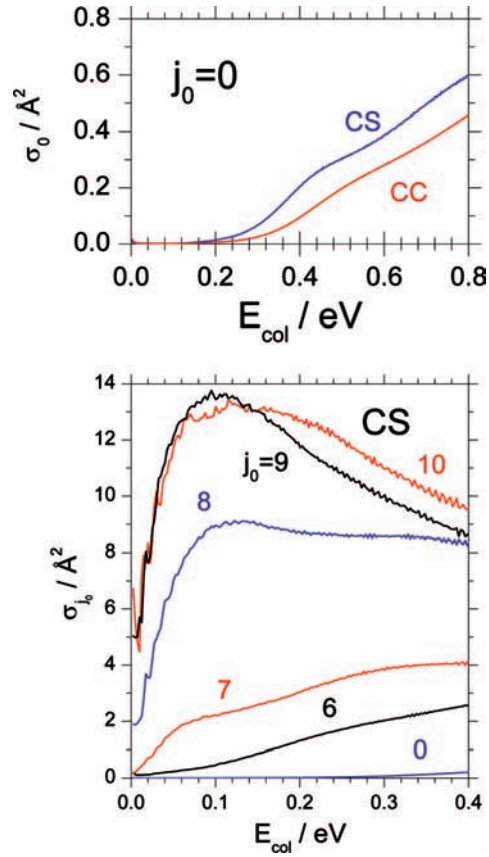

Figure 3. (Top) CC and CS cross sections σ_0 at $j_0 = 0$. (Bottom) CS cross-sections σ_{j_0} at $j_0 = 0$, 6, 7, 8, 9, and 10.

oscillating than the CC one. Overall, the σ_0 CC-CS agreement is good, although we must expect larger CS errors when HCl is rotationally excited, as probabilities of Figures 1 and 2 show. With this in mind, we plot in the lower panel of Figure 3 some CS cross sections $\sigma_{j_0}(E_{col})$ up to $E_{col} = 0.4$ eV. These results clearly show the HCl rotation enhancement on the F + HCl reactivity. For example, $\sigma_0(0.095) = 0.002$ Å^2 should be compared with the maximum value $\sigma_9(0.095) = 13.8$ Å^2, which is ~7000 times larger.

From the CS cross sections, we obtain that the CS rate constant $k(300)$ at 300 K is equal to 1.4×10^{-12} cm^3 s^{-1}, which is much smaller than the most recent experimental value[2] $k(294) = (7.2 \pm 0.3) \times 10^{-12}$ cm^3 s^{-1}. Note that previous theoretical works[3−5] matched the experimental rate only via an empirical scaling of the barrier height, from 0.174 to 0.049 eV. We thus think that nonadiabatic effects, spin−orbit couplings, and full CC calculations are necessary for a better agreement with the observed rate.

4. WP Time Evolution

We present in Figure 4 the time evolution of the r-averaged WP densities

$$\rho^0_j(R,\gamma,t) = \sin\gamma\langle\psi^0_{j_0}(R,r,\gamma,t)|\psi^0_{j_0}(R,r,\gamma,t)\rangle_r \qquad (3)$$

with $J = 0$, $j_0 = 0$ and 10, and $t = 0$, 160, 320, and 640 fs. These four snapshots show the initial WPs at $R = 16a_0$, their motion toward the interaction region, the WP collision on the PES wall, and the WPs reflected back into the reactant channel.

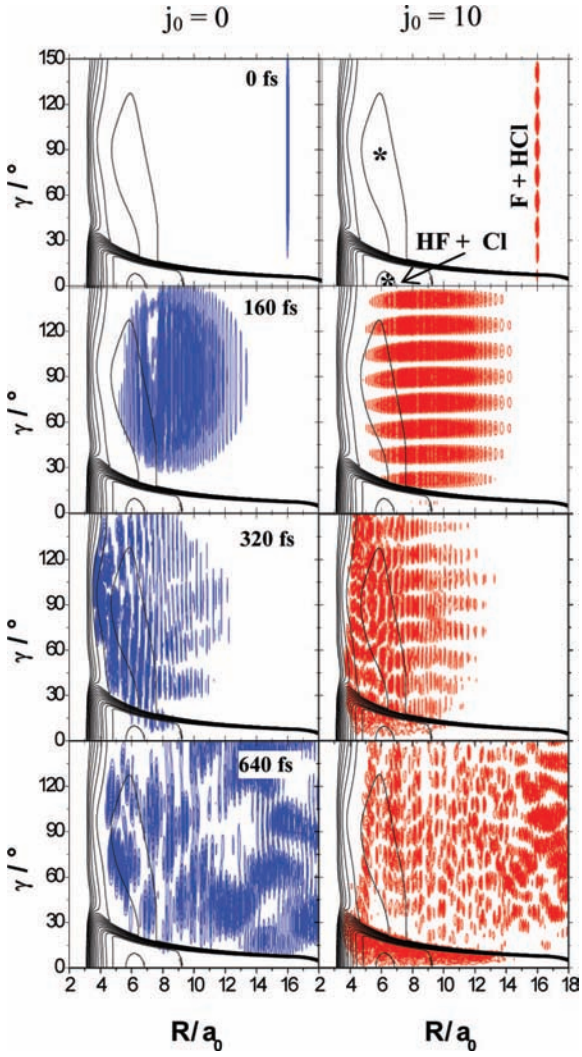

Figure 4. r-Averaged WP densities at $J = 0$ and $j_0 = 0$ and 10 superimposed on the effective potentials V_0^{eff} and V_{10}^{eff}, respectively. Snapshots at $t = 0$, 160, 320, and 640 fs. Potential values with respect to the F + HCl energy. The stars label the van der Waals minima.

The densities are superimposed on two-dimensional effective potentials at $J = 0$

$$V_{j_0}^{\text{eff}}(R,\gamma) = \min_r V(R,r,\gamma) + j_0(j_0 + 1)/2\mu_{\text{F+HCl}}R^2 \quad (4)$$

where at any (R,γ) pair we employ the minimum value of the PES $V(R,r,\gamma)$ with respect to r.

The effective potentials are very similar, owing to the large reduced mass, and are clearly shown in the panels at 0 fs. F + HCl reactants are at $R = 16a_0$ and $\gamma \geq 25°$, whereas HF + Cl products correspond to nearly collinear F−H---Cl configurations, with $R \approx$ F---Cl $\approx 7.5a_0$ and γ smaller than ∼25°. Higher γ values correspond to bent FHCl geometries, which are nonreactive, except in the immediate proximity of the transition state. The stars label the entrance and exit van der Waals minima at $R \approx 6.5a_0$, the former at $\gamma \approx 90°$ and −0.02 eV and the latter at $\gamma \approx 0$ and −1.55 eV. At any j_0, the reactive portion of the WP must thus move close to the $\gamma = 0$ FHCl linear geometry.

Superimposed on the effective potentials, we see the WP dynamics, in particular the reactive flux that enters into the product channel, at $\gamma < 25°$. At $t = 320$ and 640 fs, the left panels of Figure 4 show that the nodeless $j_0 = 0$ WP spreads

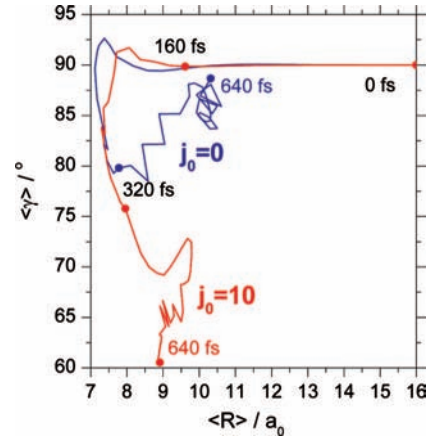

Figure 5. $(\langle R\rangle,\langle\gamma\rangle)$ trajectories at $J = 0$ and $j_0 = 0$ and 10.

far into the nonreactive γ region, where it is reflected back by the PES wall. Therefore, only a negligible $j_0 = 0$ density reaches the product configuration, and the associated reactivity is very small. On the other hand, when HCl is rotationally excited, the right panels of Figure 4 show a 10-node WP and a large reactive flux into the product channel at small γ values and $t \geq 320$ fs, in spite of the linear vanishing of the sin γ volume element of eq 3. Contrasting product channels at these j_0 values, we see that the largest difference is at 640 fs, when only the $j_0 = 10$ collision is reactive. Altogether, these results explain the j_0 enhancement of the reactivity and point out that the $1^2A'$ F + HCl reaction is highly stereospecific.

Another, even though less detailed, measure of the role of the HCl rotational excitation is given in Figure 5, which reports two trajectories of the average $(\langle R\rangle,\langle\gamma\rangle)$ values, up to 640 fs. For both $j_0 = 0$ and 10, the average angle is equal to 90° up to ∼160 fs, i.e., initially F approaches Cl independent on j_0. After ∼240 fs, F begins to move toward small γ values, i.e., toward the PES barrier and H. Then, after ∼300 fs, $\langle\gamma\rangle$ of the $j_0 = 10$ WP decreases much more than that at $j_0 = 0$, reaching a value of ∼60°, near the barrier value of 56.5°. Only the excited WP thus enters essentially into the reactive, nearly collinear, F−H−Cl surface region at small γ values. Also, this angular time evolution thus reflects the reactivity increase with j_0.

5. Conclusions

We investigated the BO dynamics of the reaction $F(^2P)$ + $HCl(X^1\Sigma^+) \rightarrow HF(X^1\Sigma^+)$ + $Cl(^2P)$, employing a recent $1^2A'$ ground-state PES and the real WP and flux methods. We calculated CC and CS reaction probabilities, cross sections, and WP densities for many rotational states of HCl in the ground vibrational state. CC and CS probabilities have been obtained up to $J = 80$ and 140, respectively, and up to $j_0 = 16$ and $K_0 = 10$.

The HCl rotational excitation increases remarkably reaction probabilities and cross sections. Also, steric effects are important, because the reactivity is enhanced by low K_0 and K values, i.e., when $\boldsymbol{j}_0$ is nearly orthogonal to the FHCl plane and H thus rotates initially in this plane, approaching the F atom. WP snapshots confirm this mechanism, showing that initially F moves straight toward Cl and then overcomes appreciably the barrier, entering the exothermic product channel, only if HCl is initially rotating. Coriolis couplings between many $|K\rangle$ states strengthen this scenario, because they inhibit or enhance the reactivity, when the initial K_0 value is small or large, respectively. Finally, the BO and CS approximations severely underestimate the room-temperature rate constant.

Acknowledgment. We thank Dr. Sinan Akpinar for many stimulating discussions. This work was supported by the Ministero per l'Istruzione, l'Università, e la Ricerca, by the Università di Siena, and by the Istituto per i Processi Chimico-Fisici del Consiglio Nazionale delle Ricerche di Pisa.

References and Notes

(1) Würzberg, E.; Houston, P. L. *J. Chem. Phys.* **1983**, *72*, 5915.
(2) Moore, C. M.; Smith, I. W. M.; Stewart, D. W. A. *Int. J. Chem. Kinet.* **1994**, *26*, 813.
(3) Sayós, R.; Hernando, J.; Francia, R.; González, M. *Phys. Chem. Chem. Phys.* **1999**, *1*, 947.
(4) Sayós, R.; Hernando, J.; Francia, R.; González, M. *Phys. Chem. Chem. Phys.* **2000**, *2*, 523.
(5) Tang, B. Y.; Yang, B. H.; Han, K. L.; Zhang, R. Q.; Zhang, J. Z. *J. Chem. Phys.* **2000**, *113*, 10105.
(6) Deskevich, M. P.; Hayes, M. Y.; Takahashi, K.; Skodje, R. T.; Nesbitt, D. J. *J. Chem. Phys.* **2006**, *124*, 224303.
(7) Hayes, M. Y.; Deskevich, M. P.; Nesbitt, D. J.; Takahashi, K.; Skodje, R. T. *J. Phys. Chem. A* **2006**, *110*, 436.
(8) Zolot, A. M.; Nesbitt, D. J. *J. Chem. Phys.* **2007**, *127*, 114319.
(9) Quéméner, G.; Balakrishnan, N. *J. Chem. Phys.* **2008**, *128*, 224304.
(10) Gray, S. K.; Balint-Kurti, G. G. *J. Chem. Phys.* **1998**, *108*, 950.
(11) Meijer, A. J. H.; Goldfield, E. M.; Gray, S. K.; Balint-Kurti, G. G. *Chem. Phys. Lett.* **1998**, *293*, 270.
(12) Hankel, M.; Balint-Kurti, G. G.; Gray, S. K. *Int. J. Quantum Chem.* **2003**, *92*, 205.
(13) Gray, S. K.; Balint-Kurti, G. G.; Schatz, G. C.; Lin, J. J.; Liu, X.; Harich, S.; Jang, X. *J. Chem. Phys.* **2000**, *113*, 7330.
(14) Miquel, I.; González, M.; Sayós, R.; Balint-Kurti, G. G.; Gray, S. K.; Goldfield, E. M. *J. Chem. Phys.* **2003**, *118*, 3111.
(15) Gamallo, P.; Defazio, P.; González, M.; Petrongolo, C. *J. Chem. Phys.* **2008**, *129*, 244307.

JP8106414